XMM-Newton observation of PSR B2224+65 and its jet

C. Y. Hui[1], R. H. H. Huang[2], L. Trepl[3], N. Tetzlaff[3], J. Takata[4], E. M. H. Wu[4] and K. S. Cheng[4]

ABSTRACT

We have investigated the pulsar PSR B2224+65 and its X-ray jet with XMM-Newton. Apart from the long X-ray jet which is almost perpendicular to the direction of proper motion, a putative extended feature at the pulsar position, which oriented in the opposite direction of the proper motion, is also suggested by this deep X-ray imaging. Non-detection of any coherent X-ray pulsation disfavors the magnetospheric origin of the X-rays observed from the position of PSR B2224+65 and hence suggest that the interpretation of pulsar wind nebula is more viable. We have also probed the origin of PSR B2224+65 and identified a runaway star, which possibly originated from the Cygnus OB9 assoication, as a candidate for the former binary companion of the neutron star's progenitor.

Subject headings: pulsar — stars: individual (PSR B2224+65) — ISM: individual objects: Guitar nebula — X-rays : stars

1. INTRODUCTION

While the signature of rotation-powered pulsars is their pulsed emission, bulk of the rotational energy is going to power a relativistic outflow of magnetohydrodynamic wind particles with Lorentz factors up to $\gamma \sim 10^8$. Although pulsar winds cannot be observed directly, their presence can be inferred through their interaction with the interstellar surroundings. If the wind reaches a termination shock, a pulsar wind nebula (PWN) is formed. The term PWN had been originally referred to the shocked emission associated with young and powerful pulsars (e.g. Crab) where the wind is effectively confined by the magnetic fields of the surrounding supernova remnants and relativistic leptons reach high energy densities which make these nebulae usually luminous synchrotron sources in the radio and X-ray regimes.

A different class of PWNe which is associated with older and less powerful pulsars is bow-shock nebulae. These nebulae are not embedded in supernova remnants but interact directly with the interstellar medium (ISM). If the pulsar has a high velocity, the nebula is confined by the ram pressure of the ISM and forms the typical bow-shock structure. The bow-shock size is determined by the balance between the wind and the ISM ram pressure. Even in this old and less powerful pulsars, there is a significant fraction of the whole pulsar spin-down power which is going to feed the pulsar wind (see Bucciantini & Bandiera 2001).

Among all the pulsars with PWNe detected, PSR B2224+65 is one of the most interesting system. This pulsar has a rotational period and a period derivative of $P \sim 0.68$ s and $\dot{P} \sim 9.6 \times 10^{-15}$ s s^{-1}, respectively. This suggests PSR B2224+65 has a spin-down age of 1.13×10^6 years. The spin parameters imply a spin-down luminosity and a surface dipole magnetic field strength of $\dot{E} \sim 1.2 \times 10^{33}$ erg s^{-1} and $B \sim 2.6 \times 10^{12}$ G respectively. Concerning its distance, while the radio dispersion measure implies a value of 1.86 kpc (cf. Cordes & Lazio 2002), Chatterjee & Cordes (2004) found that by modeling the head of the shocked emission in Hα the pulsar distance could be as close as 1 kpc.

Hui & Becker (2007) have examined its X-ray properties with the Chandra data taken in October 2000. Brief results of the same observation have also been reported by Wong et al. (2003) and Zavlin & Pavlov (2004). Despite the photon statistics is limited in this data set, the spec-

tral analysis suggests that the bulk of the X-ray emission from PSR B2224+65 is non-thermal. An independent analysis that includes also the second epoch Chandra observations taken in August-October 2006 has confirmed the non-thermal nature of the X-rays detected at the pulsar position (Johnson & Wang 2010). Nevertheless, the large frame time (i.e. 3.2 sec) of these Chandra observations do not allow us to constrain the temporal properties of the pulsar. Therefore, with the existing data, we cannot determine whether the bulk of these observed X-rays are originated from the pulsar magnetosphere or from the PWN.

The proper motion of PSR B2224+65 is among the largest in the currently known pulsar population with a transverse velocity of $v = 865(d/1 \text{ kpc})$ km s^{-1} (Harrison, Lyne & Anderson 1993). Its shock interaction with the ISM produces the most well-known *Guitar Nebula* as observed in Hα (Cordes et al. 1993). Although no evidence for the X-ray emission can be found in the region of the Hα nebula, an X-ray jet apparently associated with PSR B2224+65 has been detected by Chandra (Hui & Becker 2007; Wong et al. 2003). The most peculiar fact of this jet is that its orientation deviates by $\sim 118^\circ$ from the pulsar's proper motion direction. Its X-ray spectrum is also found to be non-thermal.

Kargaltsev & Pavlov (2008) have argued that this jet-like feature may be associated with a nearby point source instead of with PSR B2224+65. However, this possibility has been ruled out by a recent analysis of the multi-epoch Chandra observations. Johnson & Wang (2010) have found that the sharp leading edge have a proper motion consistent with that of the pulsar, which secures the association between the jet and PSR B2224+65. Different pictures have been proposed to explain this X-ray jet (e.g. Bandiera 2008; Johnson & Wang 2010). However, there is still no consensus on its nature.

To further investigate the nature of the X-rays from the position of PSR B2224+65 and its enigmatic jet, a dedicated follow-up observation with improved temporal resolution and photon statistic is needed. In this paper, we present a deep XMM-Newton observation in order to study this extreme system in details. In §2, we describe the details of the XMM-Newton observation and the data reduction. In §3 and §4, we present the results of the X-ray analysis and the search for the $\gamma-$ray emission from this system respectively. Finally, we discuss the physical implications of the observed results and search for the birth place of this fast-moving neutron star in §5.

2. X-RAY OBSERVATION WITH XMM-NEWTON

PSR B2224+65 was observed by XMM-Newton on 13-14 July 2009 (Observation ID: 0604420101) with an exposure time of 75 ks. The mean epoch of this observation is at MJD 55025. The data used in this investigation were obtained with the **E**uropean **P**hoton **I**maging **C**amera (EPIC) aboard XMM-Newton (Jansen et al. 2001). EPIC consists of two Metal Oxide Semiconductor (MOS1/2) CCD detectors (Turner et al. 2001) of which half of the beam from two of the three X-ray telescopes is reflected to. The other two halves of the incoming photon beams are reflected to a grating spectrometer (RGS) (den Herder et al. 2001). The third of the three X-ray telescopes is dedicated to expose the PN CCD detector solely (Strüder et al. 2001). The PN CCD was operated in small-window mode with a thin filter to block optical stray light. All the events recorded by PN camera are time tagged with a temporal resolution of 5.7 ms, which enable us to constrain the temporal properties of this pulsar in X-ray regime for the first time. On the other hand, the MOS1/2 CCDs were setup to operate in full-window mode with a thin filter in each camera.

The aimpoint of the satellite in this observation is RA=$22^{\rm h}25^{\rm m}52.43^{\rm s}$ and Dec=$+65^\circ35'34.0''$ (J2000). With the most updated instrumental calibration, we generate the event lists from the raw data obtained from all EPIC instruments with the tasks *emproc* and *epproc* version 9.0.0 of the XMM **S**cience **A**nalysis **S**oftware (XMMSAS version 9.0.0). Examining the raw data from the PN CCD, we did not find any timing anomaly which was observed in many of the XMM-Newton data sets (cf. Hui & Becker 2006 and references therein). This provides us with opportunities for an accurate timing analysis. We then created filtered event files for the energy range 0.5 keV to 10 keV for all EPIC instruments and selected only those events for which the pattern was between $0-12$ for MOS cameras and $0-4$ for the PN

camera. We further cleaned the data by accepting only the good times when sky background was low and removed all events potentially contaminated by bad pixels. After the filtering, the effective exposures are found to be 46 ks for each MOS camera and 32 ks for PN.

3. ANALYSIS OF XMM-NEWTON OBSERVATION

3.1. Spatial Analysis

X-ray images of the $6' \times 6'$ field around PSR B2224+65 as obtained by MOS1/2 and PN camera are displayed in Figure 1. Both image have been firstly produced with a binsize of $1''$ which is subsequently smoothed with a Gaussian with a kernel size of $\sigma = 3''$. Both the pulsar and the jet can be clearly seen.

For investigating the spatial variation of the X-ray intensity of the jet, we computed the brightness profiles along its orientation with MOS1/2 and PN data which are shown in Figure 2. We estimate the counts in the consecutive boxes with a size of $25'' \times 10''$ from the raw images with a binsize of $1^{"}$ along the jet. The orientation of these sampling regions are shown in the insets of Figure 2. To estimate the background level, we have sampled the source-free regions around PSR B2224+65 within a $6' \times 6'$ field-of-view. The average background level and its 1σ uncertainties are indicated by the horizontal solid line and dotted lines in Figure 2 respectively. Apparently, the jet extends for $\sim 2.5'$ before it falls to the estimated background level. Apart from the peak corresponds to PSR B2224+65, another peak at $\sim 70''$ from the pulsar position is also observed in both MOS1/2 and PN brightness profiles. Hereafter, we refer this as a "knot-like" feature. To determine the position of the knot-like feature on the jet, we have performed source detection individually on each EPIC data set with the aid of the XMMSAS task *edetect_chain*. The mean X-ray position inferred from this observation is RA=$22^{\rm h}25^{\rm m}42.24^{\rm s}$ Dec=$+65°36'00.0''$ (J2000) with a resultant uncertainty of $5''$ by combining the statistical errors inferred from each camera in quadrature.

To further constrain the nature of the knot-like feature, we make use of the archival data obtained by the Hubble Space Telescope (HST). Utilizing the DAOphot catalog (version 4.0) released on the *Hubble Legacy Archive*[5], we have identified a possible optical counterpart with a magnitude of $R \sim 22.31$ at RA=$22^{\rm h}25^{\rm m}42.14^{\rm s}$ Dec=$+65°36'01.2''$ (J2000) which locates within the X-ray positional uncertainty of the knot[6]. The root mean square (rms) positional uncertainty is $\sim 0.2''$ of the optical source in each coordinate based on the astrometric correction with 53 reference sources in Guide Star Catalog 2 (Lasker et al. 2008). Assuming the optical source is associated with the X-ray knot, we can probe its possible nature together with X-ray spectral analysis (see §3.2).

With the archival data obtained by Chandra X-ray Observatory, it is possible for us to place a constraint on the knot's proper motion. We utilized the **C**handra **I**nteractive **A**nalysis of **O**bservations software (CIAO 4.3) for the reanalysis. We have reprocessed all the available data of PSR B2224+65 (Obs. IDs 755; 6691; 7400) obtained by the Advanced CCD Imaging Spectrometer (ACIS) onboard Chandra with the most updated calibration CALDB (ver. 4.4.5). Different from the analysis reported by Johnson & Wang (2010) and Hui & Becker (2007), we have also applied the subpixel event repositioning during reprocessing the data in order to improve the positional accuracy of each event (cf. Li et al. 2004). For this analysis, we considered only the Obs. IDs 755 and 7400 which have an epoch separation of ~ 6 yrs. The knot can be detected in both images with a wavelet source detection algorithm. Since Johnson & Wang (2010) found that the rotation between these images is negligible, simple translational astrometric corrections have been applied. The proper motion of the knot inferred from these two frames is $\mu_{\rm RA} = -1.0 \pm 0.4$ arcsec/yrs and $\mu_{\rm RA} = 0.18 \pm 0.15$ arcsec/yrs. These errors (1σ) are computed by combining the X-ray positional errors of the knot in both frames and the corresponding astrometric uncertainties in quadrature. The error budget is dominated by the uncertainties in determining the positions of the knot. In view of the large errors, the proper motion of the knot remains unconstrained.

[5] http://hla.stsci.edu/hlaview.html

[6] The position of this optical counterpart is inferred by a HST observation performed on 2001-11-22 (Proposal ID: 9129)

The insets of Figure 1 show the $1' \times 1'$ close-up view of PSR B2224+65 in the corresponding cameras. The X-ray emission from the pulsar position appears to be slightly elongated for $\sim 8''$ behind proper motion direction as illustrated by the arrow in Figure 1. In both MOS1/2 and PN images, this putative feature apparently has the same orientation. However, the elongation of this feature is close to the edge of the spatial resolution of XMM-Newton. This has motivated us to reexamine the archival Chandra data which can offer an improved angular resolution. We produced a merged epoch X-ray image after correcting the relative astrometric offsets among each data set. The epoch-merged raw X-ray image of PSR B2224+65 is shown in Figure 3a. Figure 3b shows the X-ray brightness profile as measured by eight consecutive boxes with the orientation illustrated in the inset. Interestingly, both image and the brightness profile suggest a slight deviation from a point source with deformation toward a similar direction as observed by XMM-Newton. The extent of $\sim 3''$ is observed in the ACIS data, which can possibly be the part of the highest surface brightness, though it is not conclusive with the current data (see §5 for a further discussion).

3.2. Spectral Analysis

With the aid of the XMMSAS task *epatplot*, all the EPIC data are found to be not affected by CCD pileup. For PSR B2224+65, we extracted its source spectrum from circles with a radius of $20''$ centered at the point source position in both MOS1/2 and PN cameras respectively. This choice of extraction regions corresponds to the encircled energy fraction of $\sim 75\%$ and $\sim 80\%$ in MOS1/2 and PN respectively [7]. For the jet, we sampled its source spectrum from a $122'' \times 36''$ box centered at RA=$22^{\rm h}25^{\rm m}40.69^{\rm s}$ Dec=$+65°36'07.64''$ (J2000) and the longer side oriented 66° east from the north so as to cover the whole jet. The background spectra were extracted from the nearby regions which are source-free and with sufficient size to enable a less biased sampling. Response files were computed for all datasets by using the XMMSAS tasks *rmfgen* and *arfgen*. After the background subtraction, we have 74 ± 11 cts (MOS1), 67 ± 10 cts (MOS2), 189 ± 17 cts (PN) collected from PSR B2224+65 and 183 ± 18 cts (MOS1), 212 ± 18 cts (MOS2), 453 ± 30 cts (PN) collected from the jet respectively.

We have firstly examined the data obtained from each camera individually and found that all the spectral parameters inferred from different cameras are consistent within 1σ uncertainties. In order to tightly constrain the spectral parameters, we fitted the data obtained from three cameras simultaneously for the individual analysis of PSR B2224+65 and its jet. According to the photon statistics, we grouped each spectrum dynamically so as to achieve the same signal-to-noise rate in each dataset. The adopted spectral binning ensures a sufficiently small errors in each energy bin for better discriminating the competing scenarios. All the spectral fits were performed with XSPEC 12.6.0 in the energy range of $0.5 - 10$ keV. All the quoted errors are 1σ for 1 parameter of interest (i.e. $\Delta\chi^2 = 1.0$ above the minimum).

For PSR B2224+65, we found that a simple absorbed power-law model yields a goodness-of-fit of $\chi^2 = 3.35$ with 8 d.o.f.. Examining the power-law with different spectral binning factor, the model remains to provide a very good description of the data. The best-fit power-law model and the residuals for the pulsar spectrum are shown in Figure 4. This model yields a column density of $n_H = (1.3^{+2.2}_{-1.2}) \times 10^{21}$ cm^{-2}, a photon index of $\Gamma_X = 2.0^{+0.5}_{-0.4}$ and a normalization at 1 keV of $(6.7^{+3.8}_{-2.0}) \times 10^{-6}$ photons keV^{-1} cm^{-2} s^{-1}. We have also examined whether the X-rays from PSR B2224+65 can be described in a thermal-dominant emission scenario by fitting the spectrum with a blackbody model. The best-fit model yields a column density of $n_H < 4.6 \times 10^{20}$ cm^{-2}, a temperature of $kT = 0.5 \pm 0.1$ keV and an emitting radius of $R_{\rm bb} = (14.1^{+2.8}_{-2.3}) \times d_{\rm 1kpc}$ m, where $d_{\rm 1kpc}$ at the unit of 1 kpc. The inferred emitting region is smaller than the radius of the polar cap (i.e. $R_{\rm pc} = 175$ m) as defined by the last open field lines of a dipolar magnetic field. Also, the goodness-of-fit resulted from the best-fit blackbody model is somewhat worse ($\chi^2 = 9.28$ with 8 d.o.f.) in comparison with the power-law fit. Examining the fitting residuals, some systematic deviations are found between the observed spectrum and the best-fit blackbody model. In view of these,

[7] http://xmm.esac.esa.int/external/xmm_user_support/documentation/uhb/node17.html

the blackbody model is not favored. Therefore, we conclude that the simple absorbed power-law model is favored in modeling the observed spectrum of PSR B2224+65, which agrees with the inference drawn by Hui & Becker (2007) and Johnson & Wang (2010).

For the jet, we found that a power-law model yields a column density of $n_H = (2.7^{+1.2}_{-0.8}) \times 10^{21}$ cm^{-2}, a photon index of $\Gamma_X = 1.2 \pm 0.1$ and a normalization at 1 keV of $(9.1^{+2.3}_{-1.7}) \times 10^{-6}$ photons keV^{-1} cm^{-2} s^{-1}. The model results in a goodness-of-fit of $\chi^2 = 38.37$ with 40 d.o.f. The inferred column density from fitting the jet spectrum is consistent with that inferred from the pulsar spectrum. On the other hand, in examining whether a thermal scenario is capable to describe the observed data, we attempted to fit a thermal bremsstrahlung model to the spectrum of the jet. However, we found that it results in an unphysically high temperature of $kT \sim 180$ keV. Therefore, our investigation further supports a non-thermal origin of the X-rays from the jet.

In order to constrain the spectral properties of this system more tightly, we follow the method adopted by Johnson & Wang (2010) to jointly fit individual power-law models for the X-ray spectra of the pulsar and the jet with the column density in the individual model tied together. The results are summarized in Table 1. The joint analysis yields a column density of $n_H = (2.5^{+1.0}_{-0.7}) \times 10^{21}$ cm^{-2}. The photon index and the normalization at 1 keV for the pulsar are found to be $\Gamma_X = 2.2^{+0.2}_{-0.3}$ and $(8.3^{+2.1}_{-1.6}) \times 10^{-6}$ photons keV^{-1} cm^{-2} s^{-1} respectively. The corresponding best-fit spectral parameters for the jet are $\Gamma_X = 1.2 \pm 0.1$ and $(8.7^{+1.0}_{-1.5}) \times 10^{-6}$ photons keV^{-1} cm^{-2} s^{-1} respectively. In the energy band of $0.5 - 10$ keV, the observed flux and absorption-correct fluxes for PSR B2224+65 are found to be $(2.4^{+1.8}_{-1.0}) \times 10^{-14}$ ergs cm^{-2} s^{-1} and $(3.4^{+1.7}_{-1.0}) \times 10^{-14}$ ergs cm^{-2} s^{-1} respectively. And the observed flux and absorption-corrected flux for its jet in the same energy band are $(9.1^{+3.2}_{-2.8}) \times 10^{-14}$ ergs cm^{-2} s^{-1} and $(10.0^{+3.1}_{-2.7}) \times 10^{-14}$ ergs cm^{-2} s^{-1} respectively.

X-ray emission of the jet can possibly be powered by the energy loss of the synchrotron emitting leptons during their rides from the pulsar. If the synchrotron cooling time is less than the timescale for the flow of leptons across the feature, steepening of the photon index for the synchrotron radiation is expected along the jet. In order to investigate this possible spectral variation along the jet, we divide the extraction region for the whole jet equally into two parts along its orientation. In the following, we refer the segment closer to the pulsar as region 1 and the further one as region 2. The total photon statistics collected by three EPIC cameras for region 1 and region 2 are 379 ± 28 cts and 376 ± 26 cts respectively. For modeling the spectra of these segments, we also consider the power-law model. For a more constraining analysis, we again jointly fit the spectra of regions 1 and 2 as well as the whole jet with the column density in the individual model tied together. The results are summarized in Table 1. In this joint analysis, the X-ray spectra in both regions can be well-modeled with a power-law with a slope $\Gamma_X \sim 1.3$ and hence no variation of photon index have been found.

Since a knot-like X-ray feature along the jet is identified and a possible optical source is found within its positional uncertainty, this leads us to speculate whether this is a field object just happens to locate in the error circle by chance instead of intrinsically related to the jet. Therefore, we also attempt to examine the X-ray spectrum of this knot-like feature. Within a circular region with a radius of $15''$ centered at its nominal position (see §3.1), there are 100 ± 15 cts collected by all three EPIC cameras after background subtraction. We have examined its spectrum by fitting with various single component models which include a power-law, a thermal bremsstrahlung as well as a collisional ionization equilibrium plasma model. In view of the limited photon statistic of this feature, we simply assume the column absorption is at the level constrained in the aforementioned joint analysis (i.e. $n_H = 2.8 \times 10^{21}$ cm^{-2}). We found that all three tested models result in a similar goodness-of-fit ($\chi^2 = 18.1$ with 23 d.o.f.) and hence we are not able to discriminate these competing scenarios. We notice that all the models yield an observed flux at the level of $f_X \sim 1.5 \times 10^{-14}$ ergs cm^{-2} s^{-1} ($0.5 - 10$ keV). In the HST image, the possible optical counterpart of this feature has a magnitude of $R \sim 22.31$. This gives rise to an X-ray-to-optical flux ratio of $f_X/f_R \sim 0.77$. This value is higher than that expected for a field star which typically has a ratio of $f_X/f_{\rm opt} < 0.3$ (Maccacaro et al. 1988) but con-

forms with the expected range of an AGN which typically has a ratio of $f_X/f_{\rm opt} < 50$ (Stocke et al. 1991).

Since the nature of the knot-like feature cannot be confirmed, we have also reexamined the spectral behavior of the jet with the knot removed as if it were a background source. In particular, as the knot is located in region 1, we would like to investigate whether its removal has an effect in the spectral shape of this region. After subtracting the contribution from the knot, we re-do the joint spectral fitting of the spectra of regions 1 and 2 as well as the whole jet. The results are also summarized in Table 1. The photon indices in these two regions remain to be consistent within 1σ uncertainties. Therefore, we conclude that no evidence for spectral steepening along the X-ray jet can be found in this observation.

3.3. Temporal Analysis

3.3.1. Search for the coherent pulsation from PSR B2224+65

In order to search for X-ray pulsations from the pulsar PSR B2224+65, only the data taken from the PN small window mode with a temporal resolution of 5.7 ms can be used. We extracted 1450 counts from a circle with a radius of $20''$ centered at the radio timing position. We further selected these events within the good time intervals with the counts rate of the entire field lower than 0.02 cts/sec in order to reduce the contamination from the sky background. After filtering, a total of 523 source counts was left in our study. The photon arrival times were corrected to the solar system barycenter with the BARYCEN tool (version: 1.18; JPL DE200 Earth ephemeris) of XMMSAS.

We noticed that the pulsar has a glitch at MJD ∼54266, which is about two years before our observation (MJD 55025). Since there is no further information about the relaxation time, we then performed a detailed search for a range that cover both the post-glitch frequency as well as the extrapolated value at the mean epoch of the XMM-Newton observation. We applied the Z_n^2 statistics (Buccheri et al. 1983) with the harmonics number (n) from one to ten and the H-Test (de Jager, Raubenheimer & Swanepoel 1989) with the searching step of 1/5 corresponding Fourier width in the range of 1.4650 to 1.4652 $\rm s^{-1}$. No significant signal was detected. We also folded the light curve by using the radio spin period extrapolated for the epoch of the XMM-Newton observation. However, no meaningful light curve was obtained. The pulsar ephemeris reported from the ATNF Catalogue (Manchester et al. 2005), $f = 1.46511023680$ Hz and $\dot{f} = -2.0737 \times 10^{-14}$ $\rm sec^{-2}$ (at MJD = 54420.0) were used in our study. We further computed the upper limit of the pulsed fraction f_p by $f_p = \beta\,(N_t - N_b)\,/N_t$, where N_t and N_b are the number of total photons and the background photons respectively and β is the duty cycle. Assuming $\beta = 0.5$, we placed a 1σ upper limit for the pulsed fraction to be $\sim 8\%$.

3.3.2. Search for long-term variability from the jet

As an X-ray jet is possibly subjected to magnetohydrodynamic instability, variability has been seen in many PWN systems (e.g. DeLaney et al. 2006). In order to investigate the long-term variability from the jet, we analyse the X-ray observations of this field in different epochs. We have ignored one of the Chandra observations (Obs ID. 6691) as its short exposure (∼ 10 ks) does not provide sufficient photon statistic for this analysis. The multi-epoch spectral results are summarized in Table 2. Since the flux estimates are sensitively to the column absorption, we fixed the n_H in all observations at the value inferred from the analysis of the XMM-Newton observation as it provides a superior photon statistic in the soft band and hence put a better estimate on the n_H. Also, for the sake comparison, we compute the flux in an energy range of $0.5 - 10$ keV for all cases. We found that both observed and absorption-corrected fluxes, as well as the photon index are consistent among the observations in different epochs within 1σ uncertainties. Therefore, we do not find any evidence of the long-term spectral and flux variability.

Apart from searching for the long-term variability, we have also investigated if there is any noticeable flux variation within each individual exposure. By examining the light curves, we also do not find any evidence for the variability within each observation window.

4. SEARCH FOR $\gamma-$RAY EMISSION WITH FERMI LARGE AREA TELESCOPE

PSR B2224+65 has a spin-down age of $\sim 10^6$ yrs. It has been speculated that the accelerating regions can still be sustained in the magnetospheres of some old pulsars (e.g. Zhang et al. 2004; Hui & Becker 2007). Indeed, pulsed $\gamma-$rays with energies > 0.1 GeV have recently been detected from an old radio-quiet pulsar, PSR J1836+5925, that has a characteristic age of 1.8 million years (Abdo et al. 2010). Motivated by this discovery, we also attempt to search for the $\gamma-$ray emission from PSR B2224+65.

The continuous release of the photon data obtain in the all-sky survey with the Large Area Telescope (LAT) on board the Fermi Gamma-ray Space Telescope enables us to search for the $\gamma-$ray emission from PSR B2224+65 in MeV$-$GeV regime. In this analysis, we used the data obtained between 2008 August 4 and 2011 Oct 2. We used the Fermi Science Tools v9r23p1 package to reduce and analyze the data in the vicinity of PSR B2224+65. Only events that are classified as the "Source" class[8] were used. To reduce the contamination from Earth albedo γ-rays, we excluded events with zenith angles greater than 100°. The instrument response functions "P7SOURCE_V6" were used. Events with energies between 100 MeV and 20 GeV were used for our analysis.

With the aid of the task *gtlike*, we carried out an unbinned maximum-likelihood analysis for a region-of-interest (ROI) with a 5° radius centered on the position of PSR B2224+65 in the energy range of $0.1 - 20$ GeV. We subtracted the background contribution by including the Galactic diffuse model (gal_2yearp7v6_v0.fit) and the isotropic background (iso_p7v6source.txt), as well as all sources in the second Fermi/LAT catalog (2FGL; Abdo et al. 2011) within 10° from PSR B2224+65. We assumed a power-law spectrum for PSR B2224+65 as well as all 2FGL sources in our consideration. Making use of the model parameters resulted from the maximum-likelihood analysis, we computed the test-statistic (TS) map of $2° \times 2°$ centered at the nominal position of PSR B2224+65. The TS value[9] at the position of PSR B2224+65 is found to be ~ 40. However, we speculated that this can possibly be contributed by two previously unknown nearby $\gamma-$ray sources with their TS values of ~ 29 and ~ 38 peaked at RA=336.82° Dec=65.95° (J2000) and RA=335.25° Dec=64.98° (J2000) respectively. Appending these two additional sources in the model, we have repeated the maximum-likelihood analysis and the TS map computation. With the contribution from these two serendipitous sources subtracted, the TS value at the position of PSR B2224+65 essentially drops to zero and no residual emission can be identified in the TS map. Therefore, we conclude that we do not find any evidence for $\gamma-$ray emission from PSR B2224+65 in this study. Adopting a power-law photon index of $\Gamma = 2$, we place a 1σ upper-limit of $\sim 4 \times 10^{-12}$ erg cm^{-2} s^{-1} in $0.1 - 20$ GeV.

[8] An event class in Pass 7 (i.e. evclass=2) that provides the most suitable photon data for point source spectral analysis.

[9] TS value corresponds to the detection significance of $\sigma \approx \sqrt{\mathrm{TS}}$.

5. DISCUSSION

5.1. Nature of the X-ray emission from PSR B2224+65 & its jet

We have presented a detailed investigation of the X-ray emission from PSR B2224+65 and its jet with XMM-Newton. The non-detection of any coherent X-ray pulsation suggests that the magnetospheric origin is questionable. In the context of outer-gap model, the non-thermal pulsed X-rays are resulted from the back-flowing charge particles from the outer-gap (e.g. Cheng & Zhang 1999). Based on this model, the electromagnetic cascade developed in this flow should give rise to an X-ray photon index ≤ 2. The photon index of the X-rays from PSR B2224+65 is $2.2^{+0.2}_{-0.3}$. The best-fit value is found to larger than that expected from the magnetospheric model, though they can be reconciled within 1σ uncertainties.

On the other hand, with the deep X-ray imaging of PSR B2224+65, we have revealed an interesting feature at the pulsar position which is elongated along direction of proper motion as observed in different cameras (cf. insets in Fig. 1). Although we cannot confirm its extent unambiguously with the existing data, its orientation is interesting and worth discussing. X-ray tails have

been found to be associated with many pulsars (see Kargaltsev & Pavlov 2010 for a recent review). The tails are usually oriented in the opposite direction of pulsar motion and behind the bow-shock, therefore it is interpreted as the flow of particles coming out of the ram-pressure dominated PWN. In this scenario, the X-ray emission from PSR B2224+65 is originated from the synchrotron radiation from the wind particles accelerated at the termination shock. This is consistent with the unpulsed non-thermal emission inferred from this observation. For the synchrotron emitting leptons of Lorentz factor γ distribute as $N(\gamma) \propto \gamma^{-p}$, the observed photon index of $\Gamma \sim 2.2$ from the pulsar location is consistent with the value expected from the fast-cooling scenario, $\Gamma = (p+2)/2$, for the electron index lies within a typical range of $p \sim 2-3$ (Cheng, Taam, & Wang 2006).

This putative feature, which has an extent of $\sim 8''$ in EPIC images, should be resolved by Chandra. Nevertheless, in reexamining the archival Chandra data, its extent cannot confirm. On the other hand, the photon distribution of PSR B2224+65 in the merged Chandra image is slightly deviated from a point source with the deformation also toward the direction behind the pulsar proper motion. Although the evidence for the extended source cannot be conclusive with the existing data, the compact feature suggested by the Chandra data can possibly be the portion of the highest surface brightness. Complex structures of bow-shock PWNe have been observed in other systems. For example, XMM-Newton observation of a nearby pulsar PSR B1929+10 has revealed a long X-ray tail of several arc-minutes (Becker et al. 2006). Apart from confirming the detection of this long trail, a follow-up Chandra observation has further resolved a brighter but more compact feature with an extent of $\sim 10''$ around the pulsar (Hui & Becker 2008). For a further investigation of PSR B2224+65, a dedicated deep Chandra observation, which simultaneously provides a sub-arcsecond spatial resolution and a photon statistic comparable with this XMM-Newton observation, is the only way to confirm or refute this suggested feature.

While this compact feature is still questionable, the evidence for the $\sim 2'$ long jet is unambiguous. Although all the X-ray studies suggest its non-thermal nature, its physical origin remains to be obscure. Very recently, a collimated $\sim 9'$ long X-ray feature has been discovered from a radio-quiet $\gamma-$ray pulsar PSR J0357+3205 (De Luca et al. 2011) which is very similar to the jet of PSR B2224+65. It is interesting to compare the observed properties between these two systems. The spin-down luminosity of PSR J0357+3205, $\dot{E} \sim 6 \times 10^{33}$ erg/s, is ~ 6 times higher than that of PSR B2224+65, but it is the lowest among all known non-recycled $\gamma-$ray pulsars. The low column absorption suggests it is a nearby pulsar with a distance of only a few hundred parsec. Assuming there is no inclination with respect to the sky plane, this suggests the physical extent of the trail associated with PSR J0357+3205 at the order of ~ 1 pc which is similar to the case of PSR B2224+65. In both cases, there is no evidence of spectral variation along the feature. For a distance of 500 pc, the X-ray conversion efficiency $L_x/\dot{E}$ of its trail in $0.5-10$ keV is $\sim 10^{-3}$. Adopting a distance of 1 kpc for PSR B2224+65, $L_x/\dot{E}$ of its jet in the same energy band is found to be $\sim 10^{-2}$ which is an order larger than that for PSR J0357+3205. This might be why the jet of PSR B2224+65 can still be detected in spite of its larger distance.

Following De Luca et al. (2011), we estimate the highest achievable energy of synchrotron-radiating particles injected by PSR B2224+65. First, we assume the highest energy of the electrons/positrons can be gained is comparable with maximum potential drop in the magnetosphere, which is $\Delta\Phi = \left(3\dot{E}/2c\right)^{1/2}$ for an aligned pulsar (Goldreich & Julian 1969). Similar to the case of PSR J0357+3205, this results in a maximum Lorentz factor of $\gamma_{\rm max} \sim 10^8$. In the presence of a magnetic field, these particles will radiate synchrotron emission with characteristic frequency of $\nu_x = \gamma^2 eB/m_e c$, where $B_{\mu G}$ is the local magnetic field strength in the emission region in units of microgauss. Adopted a typical magnetic field at an order of ~ 5 μG, $\gamma_{\rm max}$ implies a synchrotron photon energy at the order of $h\nu_x \sim 5$ keV.

One difficulty for the synchrotron scenario is that it requires the Lorentz factor of the emitting particles to achieve the same order of $\gamma_{\rm max}$ so as to produce X-rays at a few keV. On the other hand, inverse Compton (IC) scattering between the relativistic particles and the relic photons appears to

be more viable in producing the observed X-rays. We note that the energy density of the relic photons is at the order of $\sim 10^{-12}$ erg cm^{-3}, which is comparable with the magnetic energy density for a field strength of $\sim 5\mu$G. Therefore the IC power cannot be ignored. In the IC scenario, the required Lorentz factor to produce ~ 10 keV photons is only at the order of $\gamma \sim 10^4$ which is much easier to achieve.

The major difficulty for explaining the X-ray jet of PSR B2224+65 in the context of PWN comes from its orientation with respect to the pulsar's proper motion. The jet protrudes from the pulsar and extends toward northwest, which makes an angle of $\sim 118^\circ$ from the proper motion direction of the pulsar (cf. Fig. 1). This peculiar orientation makes the bow-shock interpretation questionable as this scenario requires the nebular emission lies in an opposite direction of the pulsar's velocity vector. In view of this difficulty, different explanations for the nature of the jet association with PSR B2224+65 have been proposed, ranging from the magnetically confinement of relativistic particles leaking from the bow-shock (Bandiera 2008) to a picture similar to the AGN jet outflow (Johnson & Wang 2010). Nevertheless, there is no consensus on its physical origin yet.

Since the extended feature of PSR J0357+3205 is akin to that of PSR B2224+65, a comparative analysis between these two systems might provide us a deeper insight on the nature of their jets. While the distance and the proper motion direction of PSR B2224+65 are well-constrained, these are the most important parameters to be determined in further investigation of PSR J0357+3205. These would enable a more reliable estimations of its energetic and most importantly the orientation of the jet with respect to the pulsar's space velocity, which will allow us to ascertain if these two systems have a similar physical origin.

5.2. The origin of PSR B2224+65

PSR B2224+65 is certainly one of the most spectacular neutron stars regarding its motion through space as its transverse velocity, $v = 865(d/1\ \mathrm{kpc})$ km s^{-1}, is among the highest in the currently known pulsar population. On the other hand, the well measured bow shock with its inclination in the plane of the sky suggests a negligible radial velocity component (Chatterjee & Cordes 2004) which has been confirmed recently by Tetzlaff et al. (2009) who suggest the origin of PSR B2224+65 to lie within the Cygnus OB3 association or a small massive cluster nearby. This origin indicates a small radial velocity of $v_r = -21^{+81}_{-70}$ km s^{-1}. The proposed kinematic age of $\tau_{\rm kin} \approx 0.8$ Myr is consistent with a characteristic pulsar age of $\tau_{\rm char} = 1.1$ Myr (Hobbs et al. 2004; Manchester et al. 2005).

To advance the analysis we presented earlier (Tetzlaff et al. 2009), we attempt to identify a runaway star which might have been the former companion of this pulsar's progenitor star (we refer to such runaway stars as binary supernova scenario (BSS) runaways; Blaauw 1961). Therefore, we take all runaway star candidates with full kinematics from the runaway star catalogue of Tetzlaff et al. (2011) and compare the past flight paths of PSR B2224+65 and each runaway star varying the observables by performing a Monte-Carlo simulation to find close encounters between the pulsar and the runaway star. Simultaneously, we calculate the distance to possible parent associations/clusters listed in Tetzlaff et al. (2010) (for a full description of the procedure we refer to Tetzlaff et al. 2009 and Tetzlaff et al. 2010).[10]

For PSR B2224+65 we take the following data for the equatorial coordinates, right ascension α and declination δ, the distance to the Sun d and the proper motion components μ^*_α ($\mu^*_\alpha = \mu_\alpha \cos\delta$) and μ_δ (Harrison et al. 1993; Taylor & Cordes 1993; Yuan et al. 2010);

$$\begin{aligned} \alpha &= 336\overset{\circ}{.}469671,\ \delta = 65\overset{\circ}{.}593217, \\ d &= 2 \pm 1\ \mathrm{kpc}, \\ \mu^*_\alpha &= 144 \pm 3\ \mathrm{mas\ yr^{-1}},\ \mu_\delta = 112 \pm 3\ \mathrm{mas\ yr^{-1}}. \end{aligned} \quad (1)$$

Here we adopt $d = 2$ kpc for the calculation as published by Taylor & Cordes (1993) and adopt a reasonable error of 1 kpc that covers the distance inferred by Cordes & Lazio (2002) and Chatterjee

[10] PSR B2224+65 reaches a distance to the Sun larger than 3 kpc (the catalogue limit of the current runaway positions) if it is older than 1.3 Myr (assuming $v_r = 0$ km/s). Since the characteristic age (~ 1 Myr) provides an upper limit on the true age of young (few Myr) pulsars in most cases, it is well possible to identify the associated runaway star (the former companion, if it exists) among the catalogue runaway star candidates.

& Cordes (2004). Among 1703 runaway star candidates in the catalogue with full kinematic data, only nine appear to show possible close encounters with PSR B2224+65 (HIP 97359, 98773, 99283, 99580, 100308, 100409, 101186, 107418, 109393). For two of them, HIP 107418 and HIP 109393, separations between the runaway star and the pulsar are small at $\tau_{\rm kin} \approx 0$, i.e. at present; thus we exclude these two stars from our analysis.

Tracing back the seven remaining runaway stars and OB associations/ clusters listed in Tetzlaff et al. (2010), we find that four stars could have been ejected from their parent cluster within the last 3 Myr ($\approx 3 \cdot \tau_{\rm char}$) (see Table 3). For them, we simultaneously trace back PSR B2224+65, the runaway star and the potential parent association varying the observables within their confidence intervals (here we adopt $v_r = 0 \pm 100$ km s^{-1} for PSR B2224+65) to find the closest approach between the pulsar and the runaway star (i.e. the minimum separation $d_{\rm min}\,(\tau_{\rm kin})$) as well as the associated time ($\tau_{\rm kin}$) and the distance to the respective association centre at that time.

In only one case – HIP 99580 (=V2011 Cyg) with Cyg OB9 being the parent association – the pulsar and the runaway star can be located within the association boundaries (radius of Cyg OB9 ≈ 40 pc) at the same time in the past. The smallest separation $d_{\rm min}$ between PSR B2224+65 and HIP 99580 that is found after 15 million Monte-Carlo runs is 0.4 pc. Between 25 pc and 35 pc distance from the centre of Cyg OB9 [11], we find a peak of small separations $d_{\rm min}$ between the pulsar and the runaway star. In 2540 simulations the distance of the pulsar as well as the distance of the runaway star to the centre of Cyg OB9 falls within this range. The first part of the distribution of the separations $d_{\rm min}$ between PSR B2224+65 and HIP 99580 of these runs is consistent with the hypothesis that both stars once were at the same position 0.65 ± 0.05 Myr in the past (see Figure 6).

Although only a small fraction of runs yield small separations d_{min} between the stars as well as the centre of Cyg OB9 the scenario seems likely considering the errors on the parameters involved (distance d, proper motion components $\mu^*_\alpha = \mu_\alpha \cos\delta$ and μ_δ, radial velocity v_r of both stars[12]). The fraction of successful runs is much smaller than in the case of the known neutron star/ runaway pair PSR B1929+10/ ζ Ophiuchi (about one order of magnitude; for PSR B1929+10/ ζ Oph three million Monte-Carlo runs were performed approximately twice the number of successful runs compared to 15 million here; see Hoogerwerf et al. 2001 and Tetzlaff et al. 2010); however, since PSR B2224+65 and HIP 99580 are far more distant from the Sun than PSR B1929+10 and ζ Oph (the error on the distance is larger by about one to two orders of magnitude), this is to be expected.

In Figure 7, we show the correlations between the astrometric parameters which were used as input for the 2540 runs for which both, PSR B2224+65 and the runaway star HIP 99580, were situated between 25 pc and 35 pc from the centre of Cyg OB9. For the runaway star only little correlation between π and v_r can be seen and the most probable values of all parameters fall clearly within the error bars. Whereas for the pulsar there is a strong correlation between π and v_r. This is expected since an increase in distance (decrease in π) can be compensated for by a larger radial velocity v_r and vice versa. If PSR B2224+65 and the runaway star HIP 99580 were at the same place 0.65 Myr ago in Cyg OB9, i.e. once were in the same multiple system, the present distance of PSR B2224+65 needs to be ~ 0.8 kpc. Hence, we can confirm previous findings by Chatterjee & Codes (2004) which concludes the pulsar have a distance to the Sun of ~ 1 kpc.

If this supernova occurred 0.65 Myr in the past, it was located at Galactic coordinates $l = 77.4 \pm 0.2$ deg, $b = 2.5^{+0.4}_{-0.2}$ deg[13], and a distance to Earth of $d_{\rm Earth} = 968^{+32}_{-28}$ pc.

If HIP 99580 is a BSS runaway star, it should show signs of stellar evolution in the former system such as a large rotational velocity and an enhanced helium abundance caused by momentum and mass transfer during evolution. It was

[11] We choose a distance range of 10 pc to make it comparable to the previously suggested neutron star/ runaway pair PSR B1929+10/ζ Ophiuchi, see Hoogerwerf et al. (2001) and Tetzlaff et al. (2010)

[12] The errors on the motion of Cyg OB9 are also taken into account but are negligible compared to the stars.

[13] These coordinates are as viewed at the present time. (i.e. Without the correction for the Sun's motion through the Galaxy over the last 0.65 Myr.)

claimed by Barannikov (1993) that HIP 99580 is a spectroscopic binary, however De Becker & Rauw (2004)[14] and Turner et al. (2008) could not confirm this. According to Conti & Ebbets (1977), the O5 type star HIP 99580 is a rapid rotator with $v \sin i = 270$ km s^{-1}. Penny (1996) investigated $v \sin i$ of O-type stars and found that only a small number of very massive stars show such a large $v \sin i$. Hence, it is reasonable to assume that it gained its large $v \sin i$ during the earlier evolution in a binary system. Furthermore, BSS runaway stars should be blue stragglers, i.e. they appear younger, hence bluer, than their parent association (see Hoogerwerf et al. 2001 for other examples). In Figure 8 we show the colour-magnitude diagram of the potential parent association Cyg OB9 with the data adopted from Garmany & Stencel (1992). Apparently, the association consists of two major groups of different ages, the younger one being ~ 4 Myr old.[15] If HIP 99580 originated from Cyg OB9, it is clearly a blue straggler.

Assuming an association age of 4 Myr, the progenitor star of the neutron star must have been 3.4 Myr old as it exploded. Thus, its mass was (67 ± 15) $M_\odot$ (Tinsley 1980; Maeder & Meynet 1989; Kodama 1997). For such large masses, formation of black holes is expected rather than neutron stars (upper limit ≈ 30 $M_\odot$, Heger et al. 2003). However, due to mass transfer during binary evolution, even more massive stars ($\gtrsim 50-60$ $M_\odot$) may eventually produce neutron stars instead of black holes (Heger et al. 2003; Belczynski & Taam 2008). Also, more massive progenitors may also produce larger speeds of the neutron star (Burrows & Young 2000) which is consistent with the extraordinary speed of PSR B2224+65.

The authors would like to thank Ralph Neuhäuser for reading the manuscript and provide useful comments for improving its quality. CYH and LT would like to thank Albert Kong and National Tsing Hua University for the hospitality during their visit in 2010 summer. CYH is supported by the National Research Foundation of Korea through grant 2011-0023383. NT acknowledges financial support from Carl-Zeiss-Stiftung and partial support from Deutsche Forschungsgemeinschaft (DFG) in the SFB/TR-7 Gravitational Wave Astronomy. LT would like to thank DFG for financial support in project SFB TR7 Gravitational Wave Astronomy. KSC is supported by the GRF Grants of the Government of the Hong Kong SAR under HKU 7009/11P.

[14] We note that these authors quote a different radial velocity of $v_r = -23.1 \pm 8.0$ km s^{-1} for HIP 99580 compared to -44 ± 4 km/s (Kharchenko et al. 2007) that we used here. In this case, the star would still be a runaway star as it was identified also from its tangential velocity (Tetzlaff et al. 2011). However, only a tiny fraction of runs would then yield small separations between HIP 99580 and PSR B2224+65 making the BSS scenario unlikely. But note that both radial velocities can be correct if the star is a spectroscopic binary, then it would be necessary to determine the systematic radial velocity.

[15] **Note that Uyanıker et al. (2001) quote an age for Cyg OB9 of 8 Myr.**

REFERENCES

Abdo, A. A., et al. 2010, ApJ, 712, 1209

Abdo, A. A., et al. 2011, arXiv:1108.1435

Bandiera, R. 2008, A&A, 490, L3

Barannikov A. A., 1993, AstL, 19, 420

Beck, R., Shukurov, A., Sokoloff, D., & Wielebinski, R. 2003, A&A, 411, 99

Becker, W., et al. 2006, ApJ, 645, 1421

Belczynski K., & Taam R. E. 2008, ApJ, 685, 400

Blaauw, A., 1961, BAN, 15, 265

Buccheri, R., et al. 1983, A&A, 128, 245

Bucciantini, N., & Bandiera, R. 2001, A&A, 375, 1032

Burrows A., & Young T., 2000, Phys. Rep., 333, 63

Chatterjee S., & Cordes J. M., 2004, ApJ, 600, L51

Cheng, K. S., Taam, R, E., & Wang, W. 2006, ApJ, 641, 427

Cheng, K. S., & Zhang, L. 1999, ApJ, 515, 337

Conti P. S., & Ebbets D., 1977, ApJ, 213, 438

Cordes, J. M., & Lazio, T. J. W. 2002, arXiv:astro-ph/0207156

Cordes, J. M., Romani, R. W., & Lundgren, S. C. 1993, Nature, 362, 133

De Becker M., & Rauw G. 2004, A&A, 427, 995

den Herder, J. W., et al. 2001, A&A, 365, L7

de Jager, O. C., Raubenheimer, B. C., & Swanepoel, J. W. H. 1989, A&A, 221, 180

DeLaney, T., Gaensler, B. M., Arons, J., & Pivovaroff, M. J. 2006, ApJ, 640, 929

De Luca, A., et al. 2011, ApJ, 733, 104

Dickey, J. M., & Lockman, F. 1990, ARA&A, 28, 215

Garmany C. D., & Stencel R. E. 1992, A&AS, 94, 211

Goldreich, P., & Julian, W. H. 1969, ApJ, 157, 869

Harrison P. A., Lyne A. G., & Anderson B. 1993, MNRAS, 261, 113

Heger A., Fryer C. L.,Woosley S. E., Langer N., & Hartmann D. H. 2003, ApJ, 591, 288

Hobbs G., Lyne A. G., Kramer M., Martin C. E., & Jordan C. 2004, MNRAS, 353, 1311

Hoogerwerf R., de Bruijne J. H. J., & de Zeeuw P. T. 2001, A&A, 365, 49

Hui, C. Y., & Becker, W. 2008, A&A, 486, 485

Hui, C. Y., & Becker, W. 2007, A&A, 467, 1209

Hui, C. Y., & Becker, W. 2006, A&A, 454, 543

Jansen, F., et al. 2001, A&A, 365, L1

Johnson, S. P., & Wang, Q. D. 2010, MNRAS, 408, 1216

Kargaltsev, O., & Pavlov, G. G. 2010, X-RAY ASTRONOMY 2009; PRESENT STATUS, MULTI-WAVELENGTH APPROACH AND FUTURE PERSPECTIVES: Proceedings of the International Conference. AIP Conference Proceedings, Volume 1248, pp. 25-28.

Kodama T., 1997, PhD thesis, Institute of Astronomy, Univ. Tokyo

Lasker, B. M., et al. 2008, AJ, 136, 735

Li, J.Q., et al. 2004, ApJ, 610, 1204

Maccacaro, T., Gioia, I. M., Wolter, A., Zamorani, G., & Stocke, J. T. 1988, ApJ, 326, 680

Maeder A., & Meynet G. 1989, A&A, 210, 155

Manchester, R. N., Hobbs, G. B., Teoh, A., & Hobbs, M. 2005, AJ, 129, 1993

Marigo P., Girardi L., Bressan A., Groenewegen M. A. T., Silva L., & Granato G. L. 2008, A&A, 482, 883

Penny L. R. 1996, ApJ, 463, 737

Schilbach E., & Röser S. 2008, A&A, 489, 105

Schmidt-Kaler T. H. 1982, Physical parameters of the stars

Stocke, J. T., et al. 1991, ApJS, 76, 813

Strüder, L., et al. 2001, A&A, 365, L18

Taylor J. H., & Cordes J. M. 1993, ApJ, 411, 674

Tetzlaff N., Neuhäuser R., & Hohle M. M. 2011, MNRAS, 410, 190

Tetzlaff N., Neuhäuser R., Hohle M. M., Maciejewski G., 2010, MNRAS, 402, 2369

Tetzlaff N., Neuhäuser R., & Hohle M. M. 2009, MNRAS, 400, L99

Tinsley, B. M. 1980, Fundamentals of Cosmic Physics, 5, 287

Turner, M.J.L. et al. 2001, A&A, 365, L27

Turner N. H., ten Brummelaar T. A., Roberts L. C., Mason B. D., Hartkopf W. I., & Gies D. R. 2008, AJ, 136, 55

Uyanıker, B., Fürst E., Reich W., Aschenbach B., & Wielebinski R. 2001, A&A, 371, 675

Wong, D. S., et al. 2003, High Energy Process and Phenomena in Astrophysics, ed. X. D. Li, V. Trimble, & Z. R. Wang, IAU Symp., 214, 135

Yuan, J.P., Wang, N., Manchester, R. N., & Liu, Z. Y. 2010, MNRAS, 404, 289

Zavlin, V. E., & Pavlov, G. G. 2004, ApJ, 616, 452

Zhang, L., Cheng, K. S., Jiang, Z. J., & Leung, P. 2004, ApJ, 604, 317

This 2-column preprint was prepared with the AAS LaTeX macros v5.0.

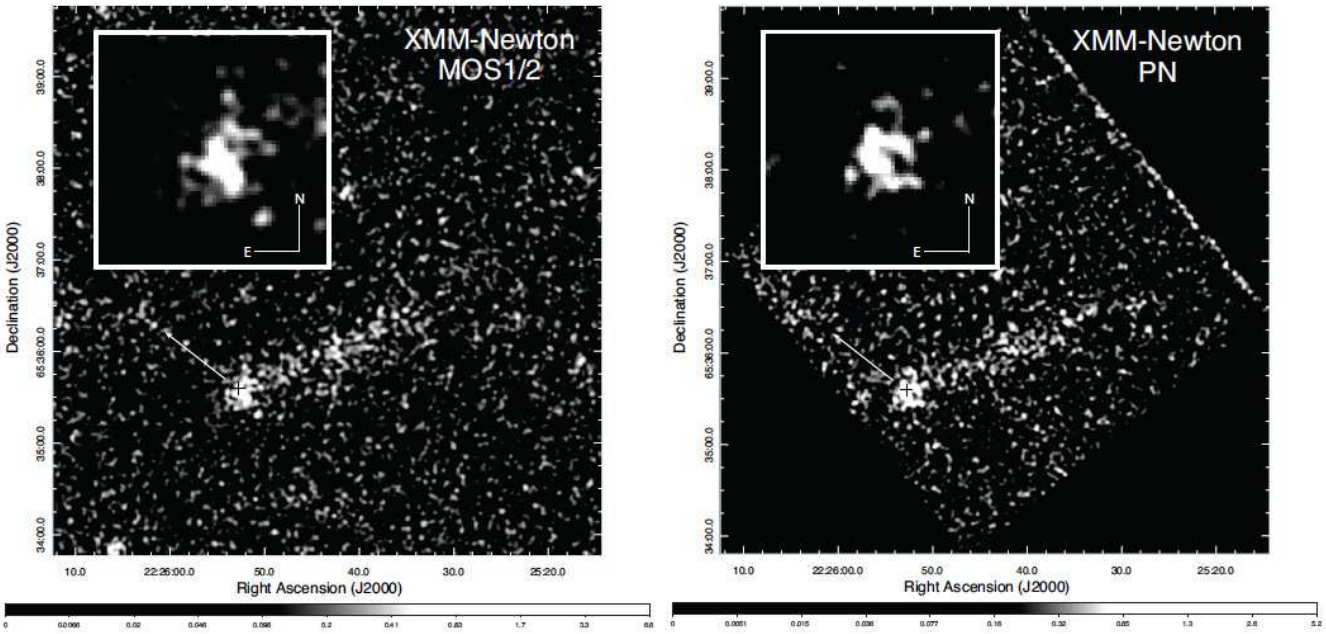

Fig. 1.— The $6' \times 6'$ field-of-view of PSR B2224+65 and its jet as observed by XMM-Newton MOS1/2 cameras (*left panel*) and PN camera (*right panel*) in the energy band of $0.5 - 10$ keV. The proper motion direction and the proper motion corrected position of the pulsar is illustrated by the black cross and white arrow respectively. The insets show the $1' \times 1'$ close-up view around PSR B2224+65. All images have been smooth by a Gaussian with $\sigma = 3''$.

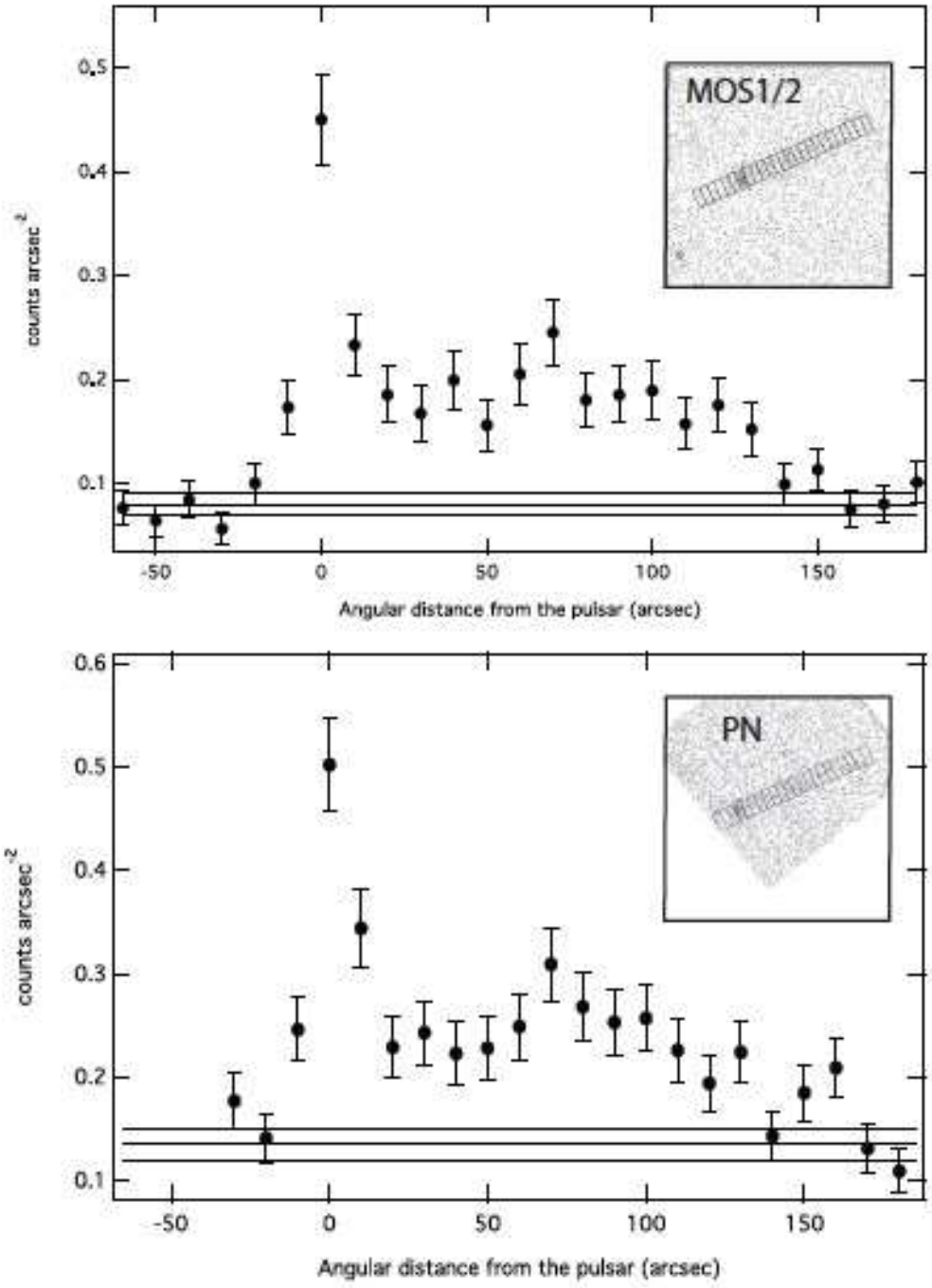

Fig. 2.— The X-ray brightness profile in the energy band of $0.5 - 10$ keV along the orientation of the jet as observed by XMM-Newton MOS1/2 cameras (*upper panel*) and PN camera (*lower panel*). The insets show the bins used in computing the profiles in the corresponding data sets. Each bin has a size of $25'' \times 10''$. The average background level and its 1σ deviation are indicated by horizontal lines which were calculated by sampling the source-free regions in the $6' \times 6'$ field-of-view of the corresponding data sets as shown in Figure 1.

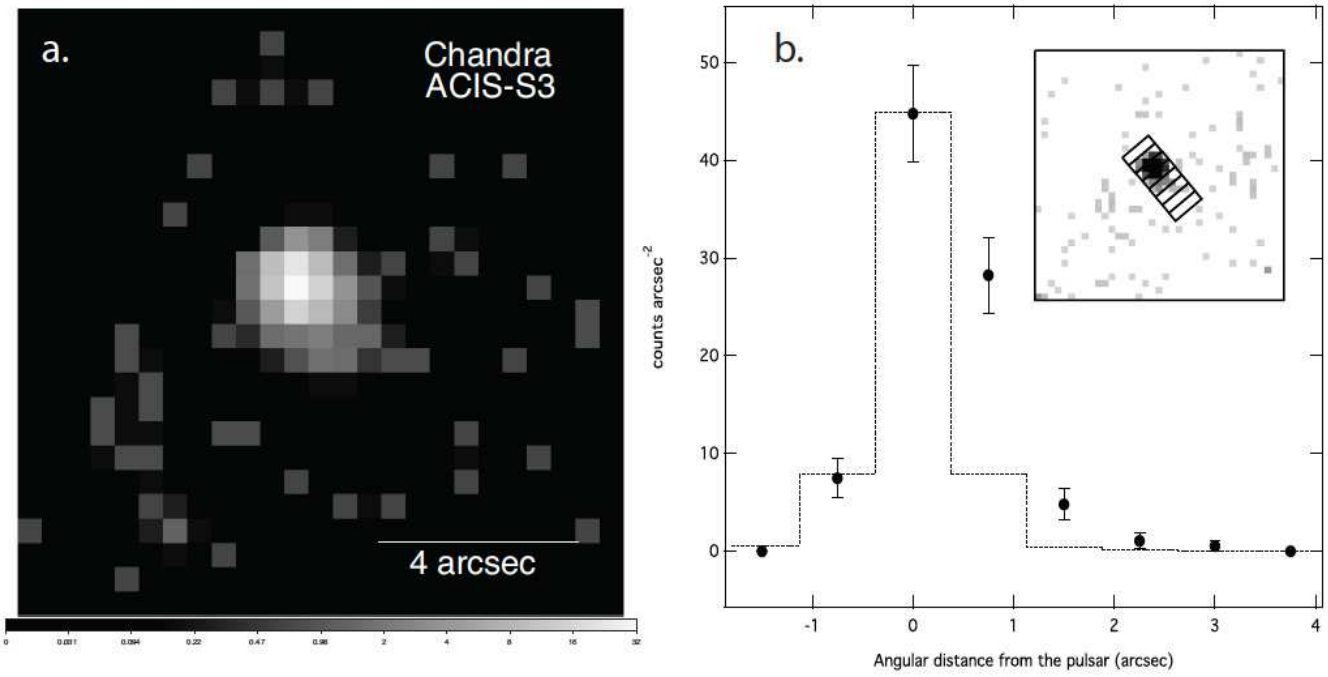

Fig. 3.— **a.** The X-ray image in the energy band $0.5 - 8$ keV centered on PSR B2224+65 by merging the Chandra ACIS data obtained in different epoch. Top is north and left is east. **b.** X-ray brightness profile in $0.5 - 8$ keV as sampled from eight bins along the orientation as illustrated in the inset. The dash line indicates the expected profile for a point source.

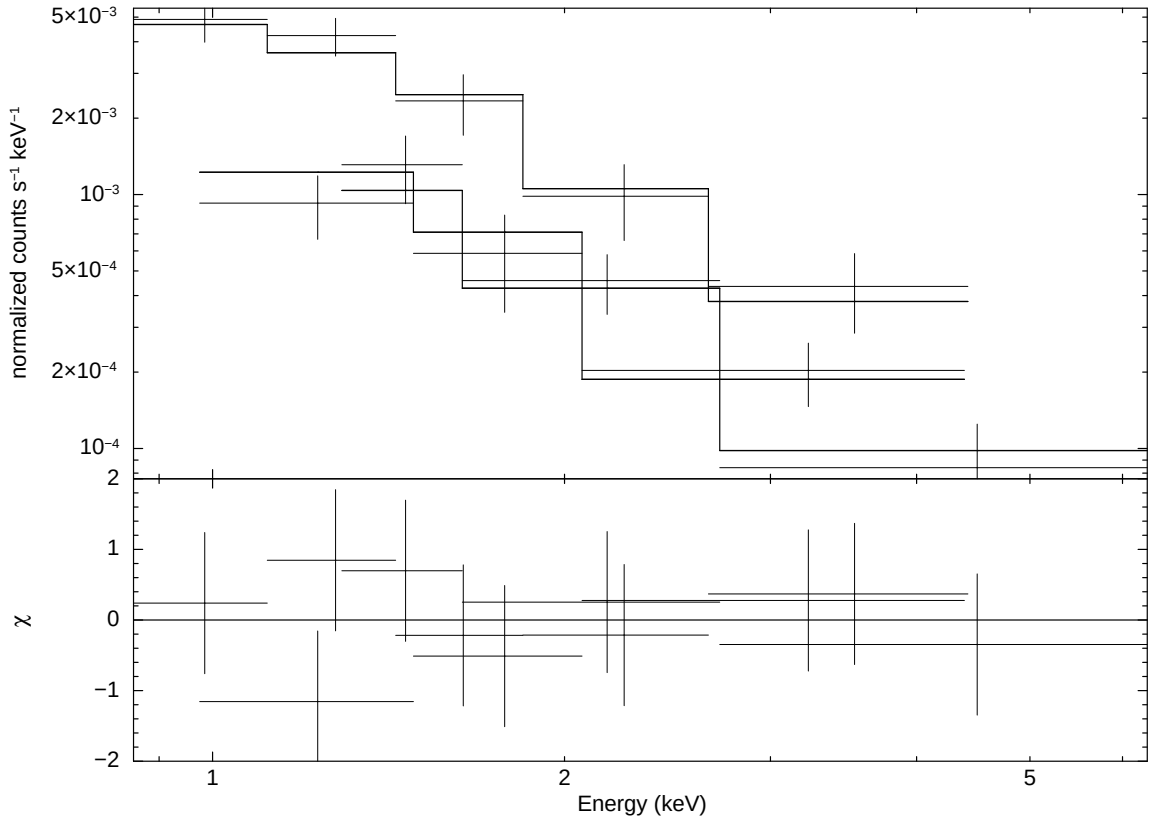

Fig. 4.— The energy spectrum of X-ray emission from the position of PSR B2224+65 as observed with the PN (upper spectrum) and MOS1/2 detectors (lower spectra) and simultaneously fitted to an absorbed power-law model (*upper panel*) and contributions to the χ^2 fit statistic (*lower panel*).

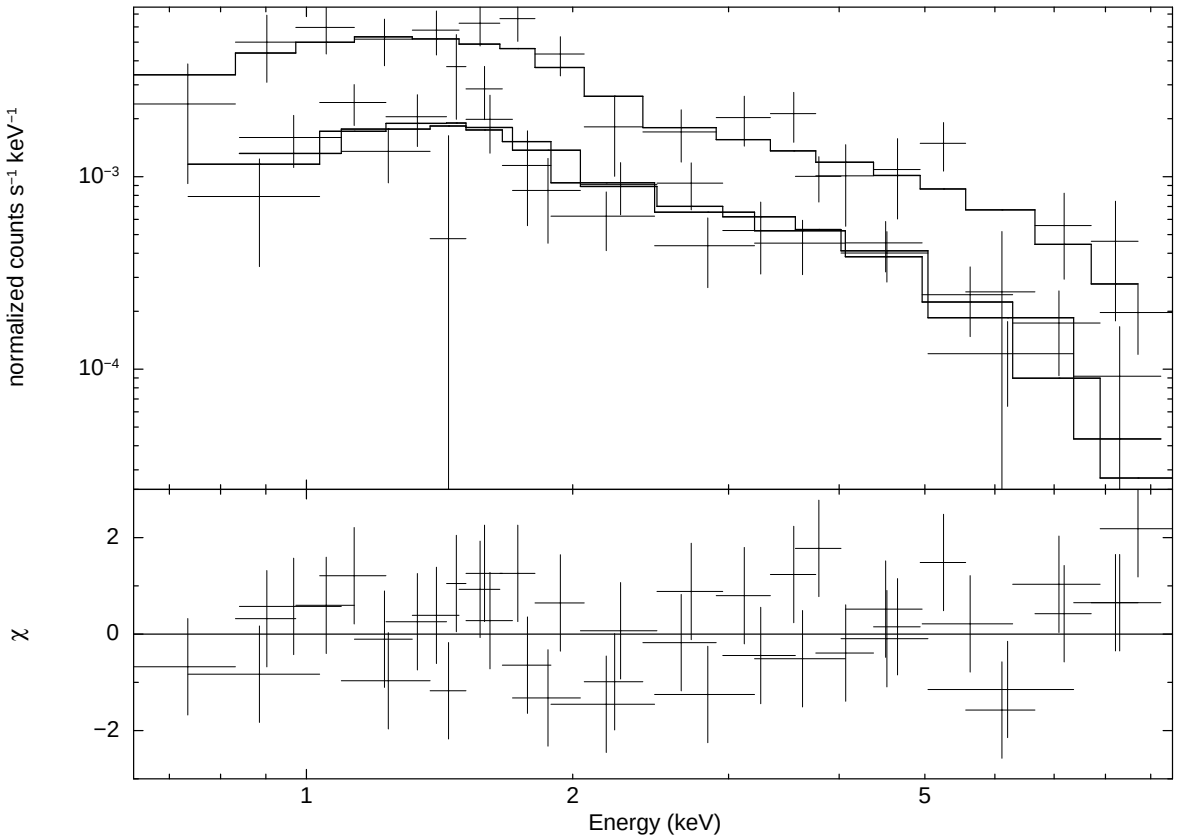

Fig. 5.— X-ray spectrum of the entire long jet feature associated with PSR B2224+65 as observed with the PN (upper spectrum) and MOS1/2 detectors (lower spectra) and simultaneously fitted to an absorbed power-law model (*upper panel*) and contributions to the χ^2 fit statistic (*lower panel*).

TABLE 1

X-RAY SPECTRAL PARAMETERS OF PSR B2224+65 AND ITS JET.[a]

Segment	n_H 10^{21} cm^{-2}	Γ_X	$f^{\rm obs}_{0.5-10\ {\rm keV}}$[b] 10^{-14} ergs cm^{-2} s^{-1}	$f^{\rm unabs}_{0.5-10\ {\rm keV}}$[b] 10^{-14} ergs cm^{-2} s^{-1}	χ^2	d.o.f
Pulsar + Whole jet						
Pulsar	$2.5^{+1.0}_{-0.7}$	$2.2^{+0.2}_{-0.3}$	$2.4^{+1.8}_{-1.0}$	$3.4^{+1.7}_{-1.0}$	42.2	49
Whole jet	...	1.2 ± 0.1	$9.1^{+3.2}_{-2.8}$	$10.0^{+3.1}_{-2.7}$	...	...
Whole jet + Region 1 + Region 2						
Whole jet	$2.8^{+0.9}_{-0.6}$	1.3 ± 0.1	$8.9^{+3.8}_{-2.5}$	$10.0^{+3.8}_{-2.5}$	86.2	91
Region 1	...	1.3 ± 0.1	$4.4^{+1.4}_{-1.5}$	$5.0^{+1.4}_{-1.6}$	...	...
Region 2	...	$1.3^{+0.2}_{-0.1}$	$4.1^{+1.6}_{-1.9}$	4.6 ± 2.0	...	...
Whole jet + Region 1 + Region 2 (with the knot removed)						
Whole jet	$3.2^{+1.0}_{-0.8}$	1.1 ± 0.2	$6.9^{+4.5}_{-3.1}$	$7.7^{+4.6}_{-3.1}$	69.2	79
Region 1	...	1.1 ± 0.2	$4.3^{+2.9}_{-1.7}$	$4.7^{+2.9}_{-1.7}$	...	...
Region 2	...	$1.3^{+0.2}_{-0.1}$	$4.6^{+2.3}_{-1.3}$	$4.6^{+2.3}_{-1.3}$	...	...

[a]Following the method adopted by Johnson & Wang (2010), these parameters are obtained from the joint analysis of the spectra of segments of interest with the column densities in the individual models tied together.

[b]$f^{\rm obs}_{0.5-10\ {\rm keV}}$ and $f^{\rm unabs}_{0.5-10\ {\rm keV}}$ represent the observed and absorption-corrected fluxes in 0.5−10 keV respectively.

TABLE 2

X-RAY SPECTRAL PROPERTIES AND THE FLUXES OF THE JET-LIKE FEATURE AT DIFFERENT EPOCHS.

Start date	Obs. ID.	n_H 10^{21} cm^{-2}	Γ_X	$f^{\rm obs}_{0.5-10\ {\rm keV}}$ 10^{-14} ergs cm^{-2} s^{-1}	$f^{\rm unabs}_{0.5-10\ {\rm keV}}$ 10^{-14} ergs cm^{-2} s^{-1}
Chandra Observations					
2000-10-21	755	2.7 (fixed)	1.1 ± 0.4	$8.7^{+16.1}_{-5.5}$	$9.5^{+16.2}_{-5.8}$
2006-10-06	7400	2.7 (fixed)	1.0 ± 0.4	$8.7^{+11.3}_{-5.0}$	$9.4^{+11.6}_{-5.3}$
XMM-Newton Observation					
2009-07-13	0604420101	$2.7^{+1.2}_{-0.8}$	1.2 ± 0.1	$9.0^{+4.7}_{-3.0}$	$10.0^{+4.7}_{-3.0}$

TABLE 3

RUNAWAY STAR CANDIDATES WITH POSSIBLE CLOSE ENCOUNTERS TO THE GUITAR PULSAR AND A POSSIBLE KINEMATIC AGE $\tau_{\rm kin,*} \lesssim 3$ MYR ($\approx 3 \cdot \tau_{\rm char}$). THE POSSIBLE PARENT ASSOCIATION AND THE ASSOCIATED $\tau_{\rm kin,*}$ ARE GIVEN IN COLUMNS 2 AND 3. COLUMNS 4 AND 5 QUOTE THE STAR'S AGE τ_* AND MASS M_* AS INFERRED FROM EVOLUTIONARY MODELS (SEE TETZLAFF ET AL. 2011). THE LAST COLUMN INDICATES THE SPECTRAL TYPE AS GIVEN IN TETZLAFF ET AL. (2011).

HIP	parent	$\tau_{kin,*}$	τ_*	M_*	SpT
		Myr	Myr	$M_\odot$	
98773	Cyg OB7	$3.0^{+1.0}_{-1.0}$	11.6 ± 0.5	15.5 ± 0.8	A2V+...
99580	Cyg OB9[a]	$1.0^{+1.0}_{-1.0}$	1.5 ± 0.5[b]	44.6 ± 5.1	O5e
100409	Cyg OB9	$3.6^{+1.4}_{-0.6}$	11.1 ± 1.1	15.5 ± 2.7	B1Ib
	Cyg OB7	$5.4^{+1.6}_{-2.4}$	...	...	...
	Cep OB6	$4.0^{+1.0}_{-1.0}$	...	...	...
101186	Cyg OB9[a]	$2.1^{+0.8}_{-1.2}$	3.9 ± 0.1	37.20.1	O9.5Ia

[a]Note that Schilbach & Röser (2008) suggested an origin for HIP 99580 and HIP 101186 in the cluster NGC 6913 2.4 Myr and 2.9 Myr ago, respectively. This cluster lies within the Cyg OB1/ Cyg OB9 region.

[b]This age does not take into account that the star might be a blue straggler. As blue straggler, its age can be consistent with 4 Myr (cf. Fig. 9).

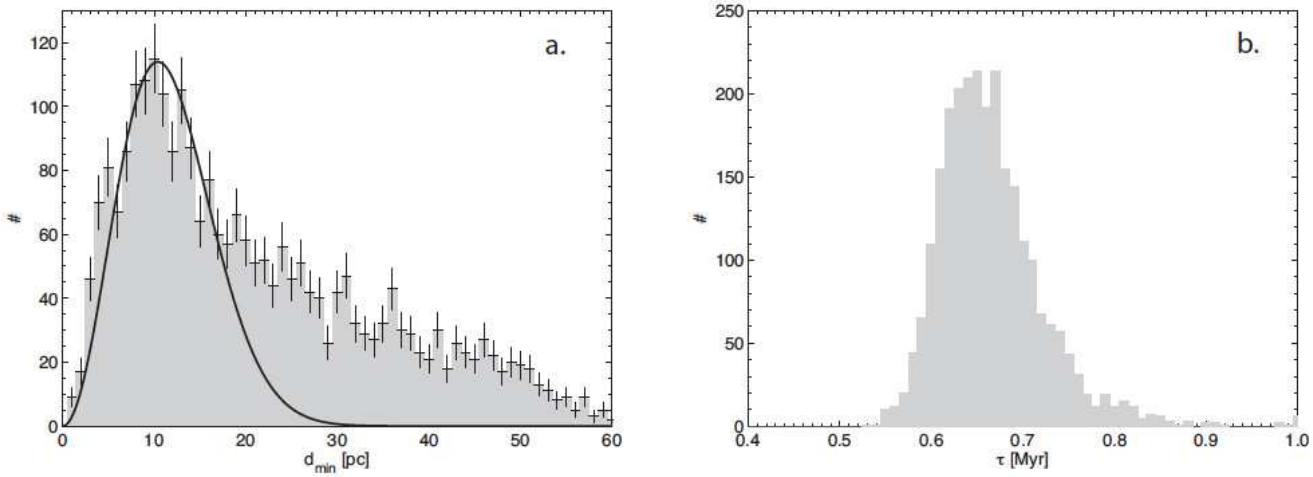

Fig. 6.— **a.** Distribution of separations $d_{\rm min}$ of the 2540 runs for which both objects, PSR B2224+65 and HIP 99580 were situated between 25 pc and 35 pc from the centre of Cyg OB9. Drawn as solid line is a theoretical curve for a distribution of absolute differences between two Gaussian distributed 3D quantities with $\mu = 0$ and $\sigma = 5.2$ pc (see equation 2 in Tetzlaff et al. 2011). **b.** Distribution of corresponding flight times τ_{kin} in the past since the SN.

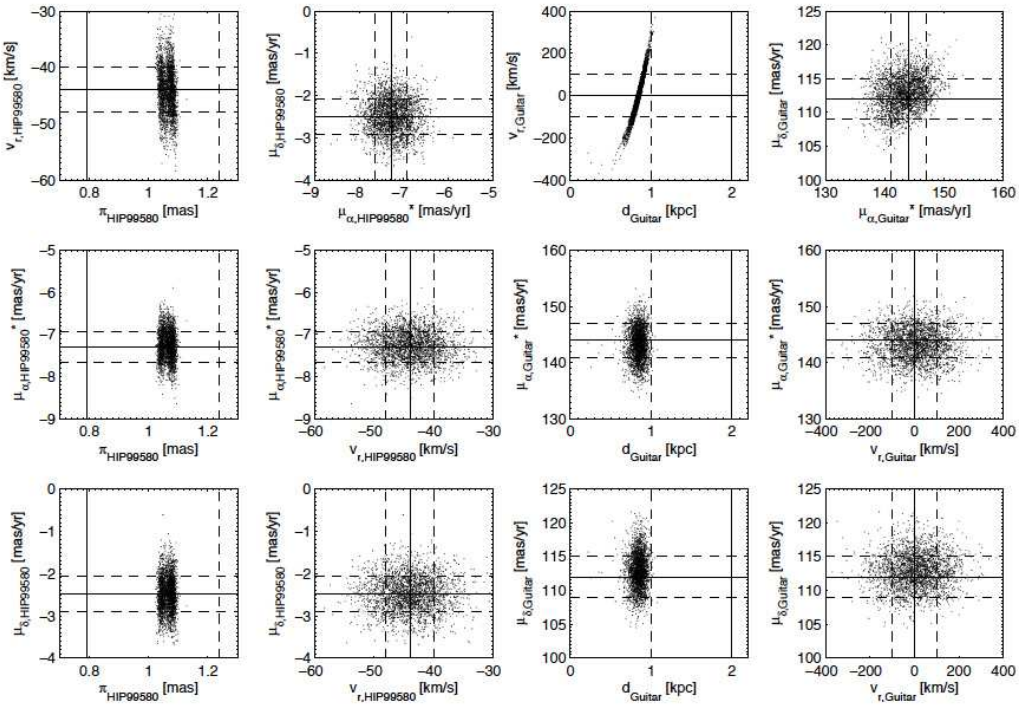

Fig. 7.— Input parameters (parallax π or distance d, proper motion components $\mu^*_\alpha = \mu_\alpha \cos\delta$ and μ_δ, radial velocity v_r) for the Guitar pulsar and the runaway star HIP 99580 for the 2540 runs for which both objects were situated between 25 pc and 35 pc from the centre of Cyg OB9. The lines mark the currently accepted parameter values (solid) and their 1σ error bars (dashed).

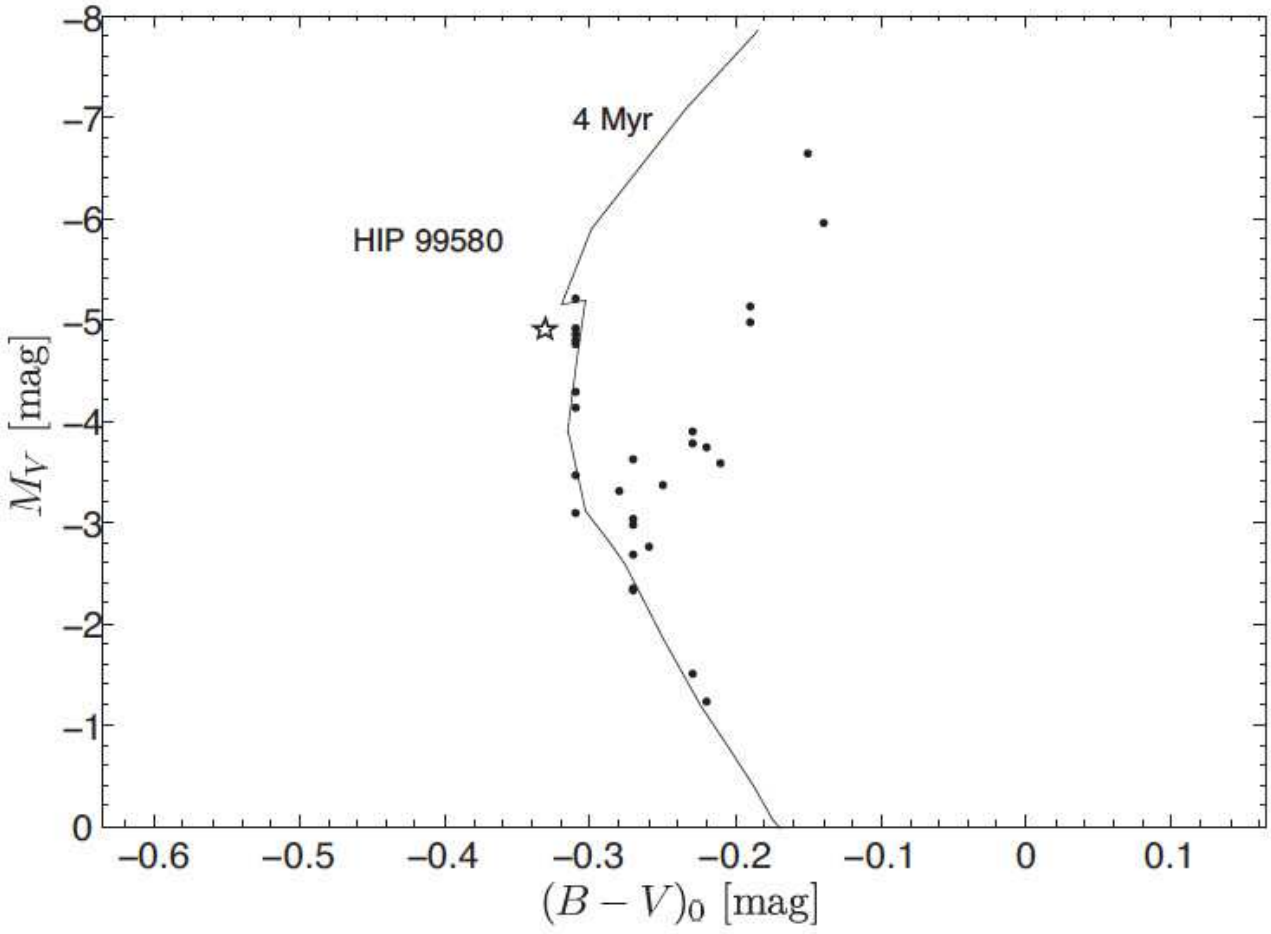

Fig. 8.— $(B-V)_0$ versus M_V diagram of Cyg OB9 (dots represent member stars according to Garmany & Stencel 1992), the potential parent association of the Guitar pulsar and the runaway star HIP 99850 (star). The solid line represents the 4 Myr isochrone from Marigo et al. (2008) (for solar metallicity; http://stev.oapd.inaf.it/cgi-bin/cmd). $(B-V)_0$ and M_V of HIP 99580 are derived from its spectral type according to Schmidt-Kaler (1982).